

# Enhancement of quantum synchronization via continuous measurement and feedback control

Yuzuru Kato<sup>1,\*</sup> and Hiroya Nakao<sup>1</sup>

<sup>1</sup>*Department of Systems and Control Engineering,  
Tokyo Institute of Technology, Tokyo 152-8552, Japan*

(Dated: April 21, 2022)

We study synchronization of a quantum van der Pol oscillator with a harmonic drive and demonstrate that quantum synchronization can be enhanced by performing continuous homodyne measurement on an additional bath linearly coupled to the oscillator and applying feedback control to the oscillator. The phase coherence of the oscillator is increased by reducing quantum fluctuations via the continuous measurement, whereas the measurement backaction inevitably induces fluctuations around the phase-locking point. We propose a simple feedback policy for suppressing measurement-induced fluctuations by adjusting the frequency of the harmonic drive, which results in enhancement of quantum synchronization. We further demonstrate that the maximum enhancement of quantum synchronization is achieved by performing quantum measurement on the quadrature angle at which the phase diffusion of the oscillator is the largest and the maximal information of the oscillator phase is extracted.

arXiv:2009.05468v1 [nlin.AO] 11 Sep 2020

---

\* Corresponding author: kato.y.bg@m.titech.ac.jp

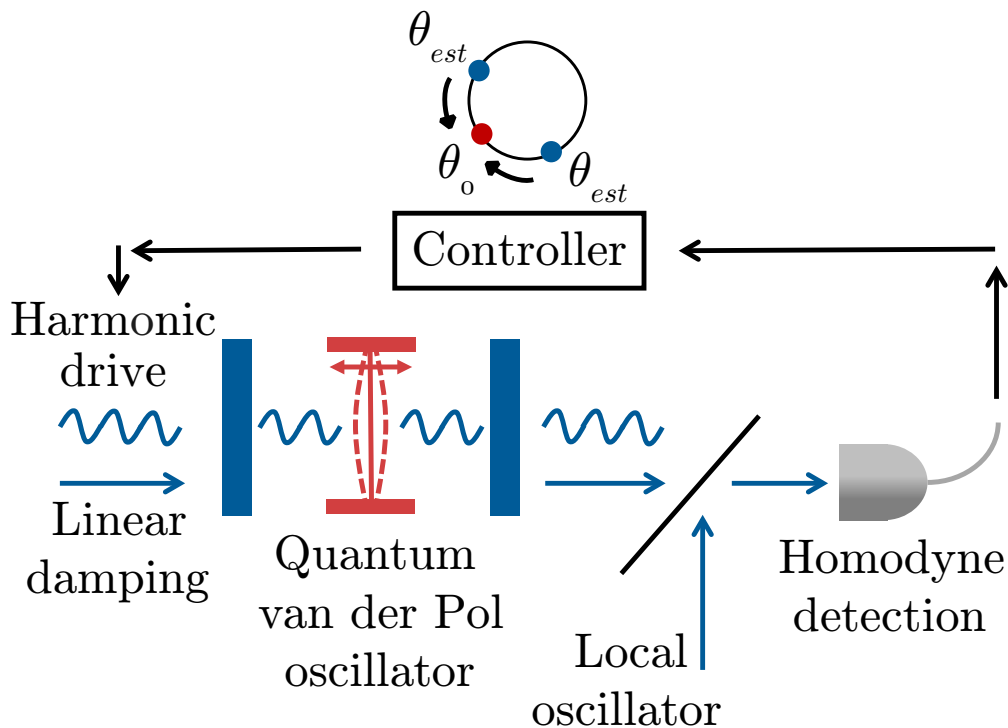


FIG. 1. Enhancement of synchronization of a quantum vdP oscillator with a harmonic drive via the continuous homodyne measurement and feedback control.

## I. INTRODUCTION

Studies pertaining to synchronization of nonlinear oscillators began in the 17th century when Huygens first documented the discovery of mutual synchronization between two pendulum clocks. Henceforth, synchronization phenomena have been widely observed in various fields of science and technology, e.g., laser oscillations, chemical oscillations, spiking neurons, chorusing crickets, and mechanical vibrations [1–5]. Furthermore, synchronization have also been analyzed in engineering applications, such as voltage standards [6], injection locking [7], phase-locked loops in electrical circuits [8], and deep brain stimulation for the treatment of Parkinson’s disease [9].

Experimental studies of synchronizing nonlinear oscillators have recently reached the micrometer and nanometer scales [10–19], and experimental demonstrations of quantum phase synchronization in spin-1 atoms [20] and on the IBM Q system [21] have been reported. Owing to these experimental developments, the theoretical analysis of quantum synchronization has received significant attention [22–44], and these studies have revealed that quantum fluctuations generally induce phase diffusion in quantum limit-cycle oscillators and disturb strict synchronization [22–26]. To overcome this deleterious effect of quantum fluctuations on synchronization, Sonar [25] applied the squeezing effect and demonstrated that the entrainment of a quantum van der Pol (vdP) oscillator to a squeezing signal can suppress quantum fluctuations, and consequently enhance quantum synchronization.

Measurement is one of the peculiar features in quantum systems; it changes the quantum state of a system depending on the probabilistic outcomes [45, 46]. When knowledge about a system is indirectly obtained by continuously monitoring the output of a field environment interacting with an open quantum system, the system dynamics under the measurement can be described by a continuous quantum trajectory, i.e., a stochastic evolution of the system conditioned by the measurement outcomes [47, 48]. This continuous measurement framework facilitates the investigation of novel dynamical features of quantum measurement, such as state preparation [49, 50], dynamical creation of entanglement [51], and unveiling [52, 53] and controlling [54] the chaotic behavior of quantum systems. It is also notable that the experimental realization of continuous measurement has been investigated recently [55–57].

Furthermore, the effect of continuous measurement of quantum limit-cycle oscillators has also been investigated, such as measurement-induced transitions between in-phase and anti-phase quantum synchronization [29], enhancement of nonclassicality in optomechanical oscillators via measurement [58], improvement in accuracy of Ramsey spectroscopy through measurement of synchronized atoms [41], characterization of synchronization using quantum trajectories

[30], and instantaneous quantum phase synchronization of two decoupled quantum limit-cycle oscillators induced by conditional photon detection [59]. However, to the best of our knowledge, the effect of continuous measurement on the enhancement of quantum synchronization has never been discussed.

In this study, we consider synchronization of a quantum vdP oscillator with a harmonic drive and demonstrate that performing continuous homodyne measurement on an additional bath linearly coupled to the oscillator and applying a feedback control to the oscillator can enhance quantum synchronization. We demonstrate that quantum fluctuations disturbing the phase coherence can be reduced by continuous homodyne measurement, and that the measurement backaction inevitably induces stochastic deviations from the phase-locking point. We propose a simple feedback policy that can suppress the fluctuations by adjusting the frequency of the harmonic drive. Furthermore, we demonstrate that the maximal enhancement of quantum synchronization can be achieved by performing the measurement on the quadrature angle at which the phase diffusion of the oscillator is the largest and the maximal information on the phase of the oscillator can be obtained via the measurement. Using measurement and feedback control, the proposed method yields more significant enhancement of phase coherence than that achieved by optimizing the waveform of the periodic amplitude modulation of the driving signal in the feed-forward setting analyzed in our previous study [27].

## II. MODEL

We consider a quantum vdP oscillator subjected to a harmonic drive. A schematic diagram of the physical setup is shown in Fig. 1. We introduce an additional linear bath coupled to the oscillator, perform continuous homodyne measurement of the output field from the oscillator to the bath, and apply a feedback control to adjust the frequency of the harmonic drive (Fig.1).

We denote by  $\omega_0$  and  $\omega_d$  the frequencies of the quantum vdP oscillator and harmonic drive, respectively. Under the assumption that the Markov approximation can be employed, the stochastic master equation of the quantum system in the coordinate frame rotating with the frequency  $\omega_d$  is written as [22, 23, 26]

$$\begin{aligned} d\rho = & \left\{ -i [ -(\Delta + \Delta_{fb})a^\dagger a + iE(a - a^\dagger), \rho ] + \gamma_1 \mathcal{D}[a^\dagger]\rho + \gamma_2 \mathcal{D}[a^2]\rho \right. \\ & \left. + \gamma_3 \mathcal{D}[a]\rho \right\} dt + \sqrt{\eta\gamma_3} \mathcal{H}[ae^{-i\theta}] \rho dW, \\ dY = & \sqrt{\eta\gamma_3} \text{Tr}[(ae^{-i\theta} + a^\dagger e^{i\theta})\rho] dt + dW, \end{aligned} \quad (1)$$

with  $\mathcal{D}[L]\rho = L\rho L^\dagger - \frac{1}{2}(L^\dagger L\rho + \rho L^\dagger L)$ ,  $\mathcal{H}[L]\rho = L\rho + \rho L^\dagger - \text{Tr}[(L + L^\dagger)\rho]\rho$ , where  $\mathcal{D}$  is the Lindblad form and  $\mathcal{H}[ae^{-i\theta}]$  characterizes the measurement on the quadrature  $ae^{-i\theta} + a^\dagger e^{i\theta}$ ,  $\rho$  is the density matrix representing the system state,  $a$  and  $a^\dagger$  denote the annihilation and creation operators ( $\dagger$  represents Hermitian conjugate), respectively,  $\Delta = \omega_d - \omega_0$  is the frequency detuning of the harmonic drive from the oscillator,  $\Delta_{fb}$  is the feedback control to adjust the frequency detuning, i.e., the frequency of the harmonic drive,  $E$  is the intensity of the harmonic drive,  $\gamma_1$ ,  $\gamma_2$ , and  $\gamma_3$  represent the decay rates for the negative damping, nonlinear damping, and linear damping, respectively,  $\eta$  is the efficiency of the measurement (we set  $\eta = 1$  when the measurement is performed, and  $\eta = 0$  when it is not),  $\theta$  specifies the quadrature angle of the measurement,  $W$  represents a Wiener process satisfying  $\mathbb{E}[dW] = 0$  and  $\mathbb{E}[dW^2] = dt$ ,  $Y$  is the output of the measurement result, and the reduced Planck's constant is set as  $\hbar = 1$ .

In the following, we use the parameter settings such that the oscillator is synchronized with the harmonic drive and the Wigner distribution, a quasiprobability distribution [60], of the steady-state density matrix  $\rho_{ss}$  of Eq. (1) is concentrated around a stable phase-locking point along the limit-cycle orbit in the classical limit (see, e.g., Fig. 3(a)) when the measurement is not performed ( $\eta = 0$ ).

We set the feedback control  $\Delta_{fb}$  as (see Appendix 1 for details)

$$\Delta_{fb} = -K_{fb}(\theta_{est} - \theta_0), \quad (2)$$

where  $K_{fb}$  ( $> 0$ ) represents the feedback gain and  $\theta_0 = \arctan(\text{Tr}[p\rho_{ss}]/\text{Tr}[x\rho_{ss}])$  represents the locking phase in the absence of the measurement, which is calculated as the angle between the expectation values of the position operator  $x = (a + a^\dagger)/2$  and the momentum operator  $p = -i(a - a^\dagger)/2$  with respect to the steady-state  $\rho_{ss}$  of Eq. (1) without measurement, and  $\theta_{est} = \arctan(\text{Tr}[p\rho_{est}]/\text{Tr}[x\rho_{est}])$ , which is chosen such that  $-\pi + \theta_0 \leq \theta_{est} < \theta_0 + \pi$ , represents the phase of the system calculated from the instantaneous state  $\rho_{est}$  of Eq. (1) with measurement, which is conditioned on the measurement record. The feedback control above can actually suppress the fluctuations of the system state around the phase-locking point as will be shown in the next section.

To evaluate the phase coherence of the quantum vdP oscillator, we use the order parameter [29, 32]

$$S_1 = |S_1| e^{i\phi_1} = \frac{\text{Tr}[a\rho]}{\sqrt{\text{Tr}[a^\dagger a\rho]}}, \quad (3)$$

which is a quantum analog of the order parameter for a single classical noisy oscillator [2, 3]. The absolute value  $|S_1|$  quantifies the degree of phase coherence and assumes the values in  $0 \leq |S_1| \leq 1$ , where  $|S_1| = 1$  when the oscillator state is perfectly phase-coherent and  $|S_1| = 0$  when the state is perfectly phase-incoherent. Note that  $\phi_1$  represents the average phase value of the oscillator.

### III. RESULTS

Numerical simulations of Eq. (1) are performed. In Sections III A, III B, and III C, we set the parameter values in the semiclassical regime,  $(\Delta, \gamma_2, \gamma_3, E)/\gamma_1 = (0.05, 0.05, 0.1, \sqrt{0.1})$ , to clarify the relation between the quantum system and its classical limit [26], and the feedback gain is set as  $K_{fb}/\gamma_1 = 1$  when we apply the feedback control. In Secs. III D, we discuss the applicability of the proposed method in the quantum regime with parameter values  $(\Delta, \gamma_2, \gamma_3, E)/\gamma_1 = (0.05, 0.25, 0.25, \sqrt{0.1})$ , and apply feedback control with a feedback gain  $K_{fb}/\gamma_1 = 7.5$ . In Sections III A, III B, and III D, we set  $\theta = 0$  for the quadrature of measurement and, in Section III C, the effect of varying  $\theta$  is analyzed. We always set the initial state of the simulation as the vacuum state, i.e.,  $\rho = |0\rangle\langle 0|$ .

#### A. Without feedback control

We first consider the case without feedback control, i.e.,  $K_{fb} = 0$ , in the semiclassical regime. When the measurement is performed, we calculated the average values over 300 trajectories obtained by the numerical simulations of Eq. (1) from the same initial state ( $\rho = |0\rangle\langle 0|$ ) because the system trajectories behaved stochastically. The average results are compared with the results in the case without measurement when the system trajectory of Eq. (1) is deterministic.

Figures 2(a), 2(b), 2(c), and 2(d) show the trajectories of the absolute values of the order parameter  $|S_1|$  quantifying the degree of phase coherence, the purity  $P = \text{Tr}[\rho^2]$ , the expectation value of the position operator  $\langle x \rangle = \text{Tr}[x\rho]$ , and the expectation value of the momentum operator  $\langle p \rangle = \text{Tr}[p\rho]$ , respectively. Note that these expectation values are fluctuating in the case with measurement.

As shown in Fig. 2(a), the average value of the order parameter  $|S_1|$  with measurement is larger than the (deterministic) value of  $|S_1|$  without measurement, e.g.,  $|S_1| = 0.859$  with measurement and  $|S_1| = 0.737$  without measurement at  $t = 250$ , signifying the phase coherence increased on average due to the continuous homodyne measurement. The increase in the purity is evident in Fig. 2(b); the average values of the purity  $P$  with measurement are larger than the stationary value of  $P$  without measurement, e.g.,  $P = 0.258$  with measurement and  $P = 0.169$  without measurement at  $t = 250$  sufficiently after the initial relaxation.

We note that the observed increase in  $|S_1|$  or  $P$  is an average effect; the values of these quantities for a single trajectory of Eq. (1) with the measurement fluctuates significantly and occasionally take smaller values than those without measurement, as shown by the dark gray lines in Figs. 2(a) and 2(b). We also note that the increase in the purity implies the reduction in the phase diffusion of the oscillator (See Appendix 2). Owing to the increase in phase coherence by the measurement, the measurement backaction inevitably induces fluctuations in the system state around the phase-locking point. It is evident from Figs. 2(c) and 2(d) that 10 trajectories of  $\langle x \rangle$  and  $\langle p \rangle$  obtained by simulating Eq. (1) with measurement (gray lines) exhibit strong fluctuations based on the measurement outcomes.

The increase in phase coherence by the measurement is also observed in the Wigner distribution. Figure 3(a) shows the steady-state Wigner distribution obtained from Eq. (1) without measurement ( $\rho$  converges to a steady state in this case), and Figs. 3(b), 3(c), and 3(d) show the instantaneous Wigner distributions at  $t = 250$  of three trajectories obtained by simulating Eq. (1) with measurement ( $\rho$  behaves stochastically in this case). Comparing Figs. 3(b), 3(c), and 3(d) with Fig. 3(a), increase in phase coherence by the continuous homodyne measurement is observed from the strongly concentrated Wigner distributions. We also observe that the location of the distribution differs by trajectory because the measurement backaction randomly disturbs the system state based on the measurement outcomes.

#### B. With feedback control

As presented in Section III A, we observed that the measurement increases phase coherence but induces fluctuations in the system state around the phase-locking point simultaneously. To suppress the fluctuations of the system state, we introduce the feedback control expressed in Eq. (2).

Figures 4(a), 4(b), 4(c), and 4(d) show the trajectories of  $|S_1|$ ,  $P$ ,  $\langle x \rangle$ , and  $\langle p \rangle$ , respectively. The feedback control is applied from  $t = 100$ . As shown in Fig. 4(a), the average order parameter  $|S_1|$  with measurement takes larger values than  $|S_1|$  without measurement, e.g.,  $|S_1| = 0.889$  with measurement and  $|S_1| = 0.737$  without measurement

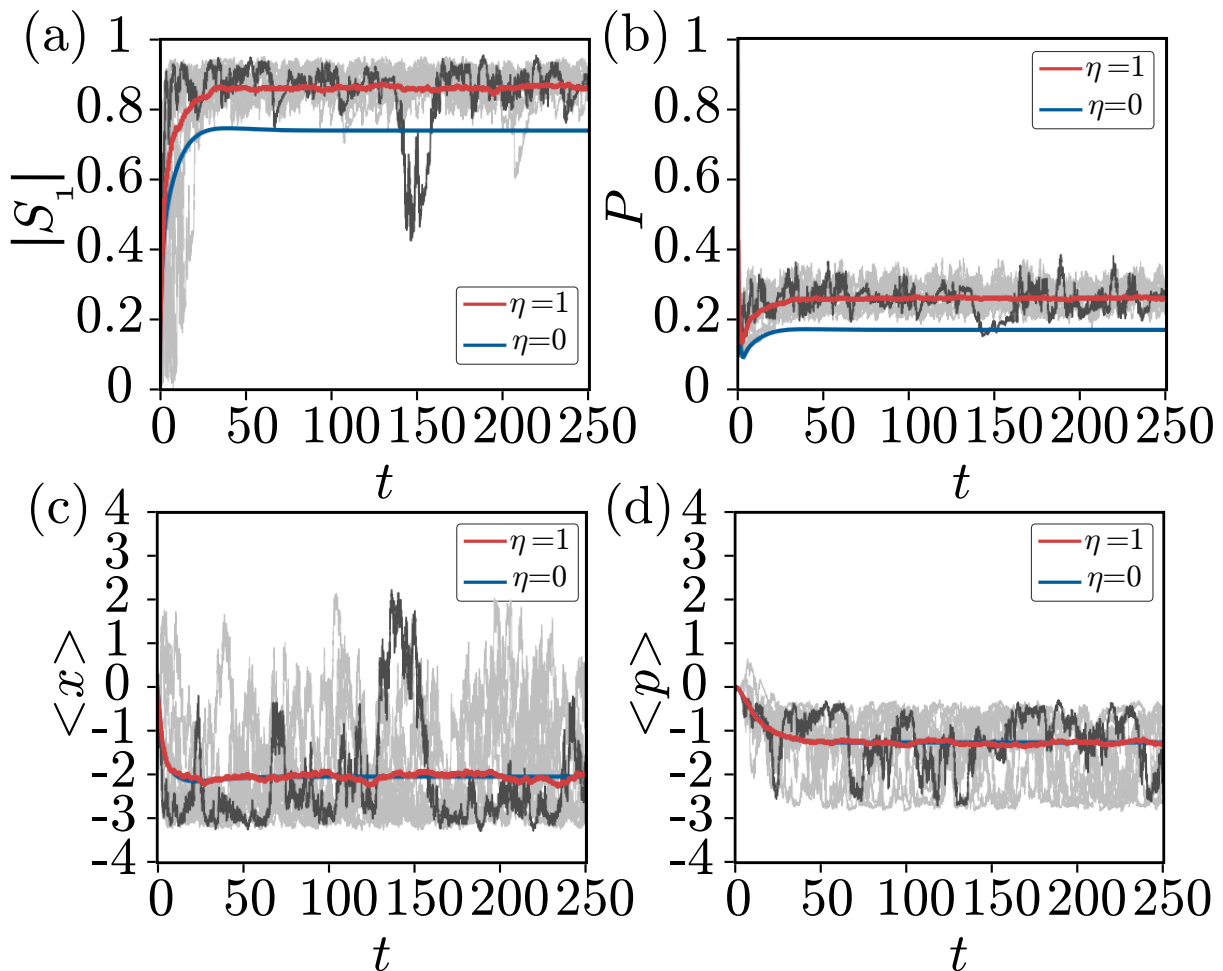


FIG. 2. Measurement-induced increase in phase coherence without feedback control in semiclassical regime. (a) Order parameter  $|S_1|$ . (b) Purity  $P$ . (c) Expectation values of position operator  $\langle x \rangle$ . (d) Expectation values of momentum operator  $\langle p \rangle$ . For the case with measurement ( $\eta = 1$ ), average values of results calculated from 300 trajectories are shown by red lines and 10 out of 300 individual trajectories are shown by gray lines, with the dark one representing a single realization of the trajectory. For the case without measurement ( $\eta = 0$ ), the results of a single trajectory are shown by blue lines.

at  $t = 250$ . We also see in Fig. 4(b) that the average values of  $P$  with measurement are larger than those without measurement, e.g.,  $P = 0.275$  with measurement and  $P = 0.169$  without measurement at  $t = 250$ .

The role of the feedback control is evident from Figs. 4(c) and 4(d), where 10 trajectories of  $\langle x \rangle$  and  $\langle p \rangle$  obtained by simulating Eq. (1) with measurement are shown (gray lines). The fluctuations around the phase-locking point are suppressed by the feedback control that is turned on after  $t = 100$ . We note that we used the same sequences of the Wiener increments in the numerical simulations of Eq. (1) in the case without feedback control.

The average values of  $\langle x \rangle$  and  $\langle p \rangle$  (red lines) are smaller than those for the case without measurement (blue lines). This can be explained as follows. The backaction induces strong fluctuations in  $\langle x \rangle$  because the measurement is performed on  $2x = (a + a^\dagger)$  with  $\theta = 0$ . Without feedback control,  $\langle x \rangle$ , which fluctuates near the phase-locking point, occasionally exhibits a large increase along the limit-cycle trajectory to the clockwise direction. This large increase in  $\langle x \rangle$  is suppressed by the feedback control, which results in a smaller average value of  $\langle x \rangle$ . Although the backaction is weaker for  $\langle p \rangle$ , the suppression of large increase in  $\langle x \rangle$  by the feedback control results in a smaller average value of  $\langle p \rangle$ .

The effect of feedback control for suppressing the fluctuations of the system state is also evident from the Wigner distribution of the system. Figure 5(a) shows the steady-state Wigner distribution of Eq. (1) without measurement, whereas Figs. 5(b), 5(c), and 5(d) show three realizations of the Wigner distributions at  $t = 250$  of Eq. (1) with measurement. Comparing Figs. 5(b), 5(c), and 5(d) with Figs. 3(b), 3(c), and 3(d), it is clear that the fluctuations

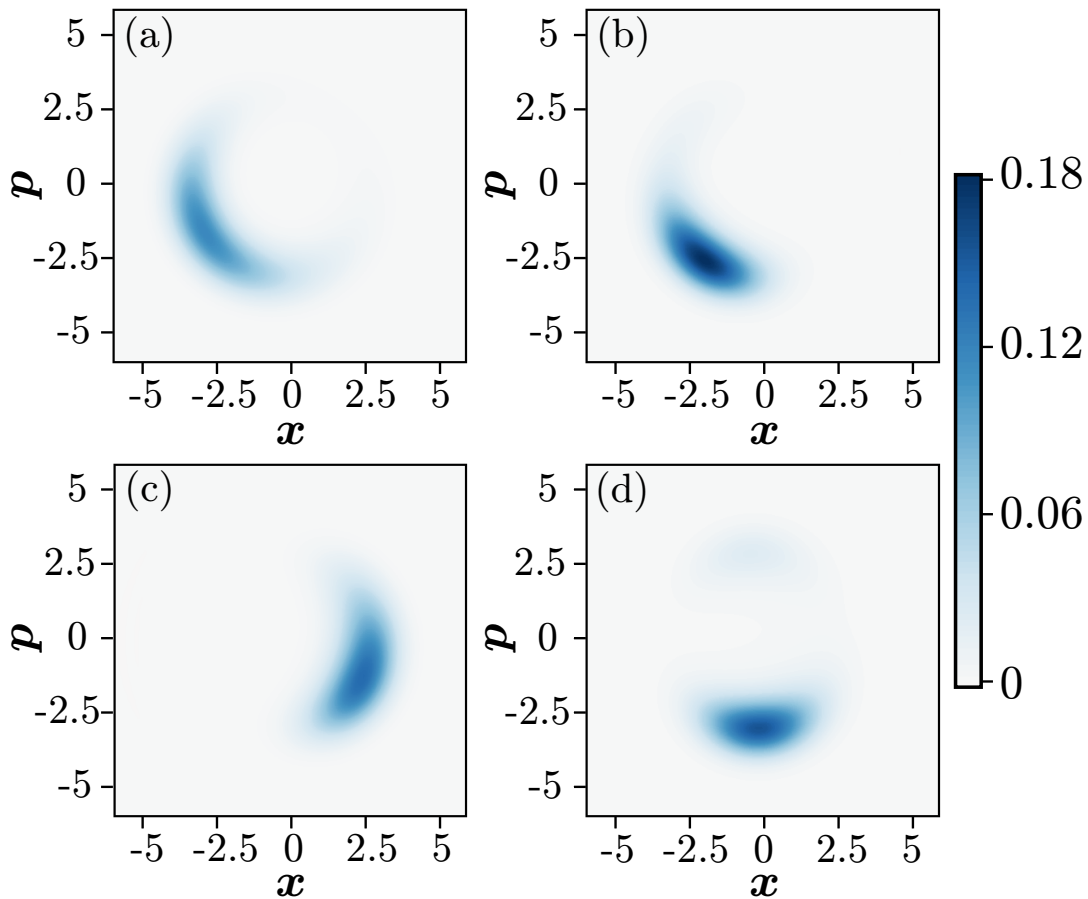


FIG. 3. Wigner distributions of system without feedback control in semiclassical regime. (a) Wigner distribution of steady state of Eq. (1) without measurement. (b,c,d) Wigner distributions of three different trajectories of Eq. (1) with measurement at  $t = 250$ .

around the phase-locking point are suppressed effectively by the feedback control.

The results above indicate that enhancement of synchronization, i.e., larger phase coherence and smaller fluctuations around the phase-locking point, can be achieved via continuous measurement and feedback control.

### C. Dependence on measurement quadrature

Thus far, we have fixed  $\theta$ , the quadrature of the measurement, at 0. Next, we consider the effect of varying  $\theta$  on the enhancement of quantum synchronization.

Figures 6(a) and 6(b) show the average values of  $|S_1|$  and  $P$  at  $t = 250$  for  $0 \leq \theta \leq 2\pi$ , respectively, which are calculated from 400 trajectories of Eq. (1) with measurement and the feedback control. For comparison, we also show the values of  $|S_1|$  and  $P$  for the steady state of Eq. (1) without the measurement. The maximum values of  $|S_1|$  and  $P$  are achieved at  $\theta = 2.199$ , which is approximately orthogonal to the locking phase, i.e.,  $\theta_0 = 3.696$ .

The result above can be interpreted as follows. The phase diffusion of the oscillator is maximized when  $\theta$  is orthogonal to  $\theta_0$ , and performing the measurement on the quadrature specified by this  $\theta$  extracts the maximum information regarding the oscillator phase. Hence, the maximum reduction in quantum fluctuations and enhancement in synchronization are attained at the quadrature angle.

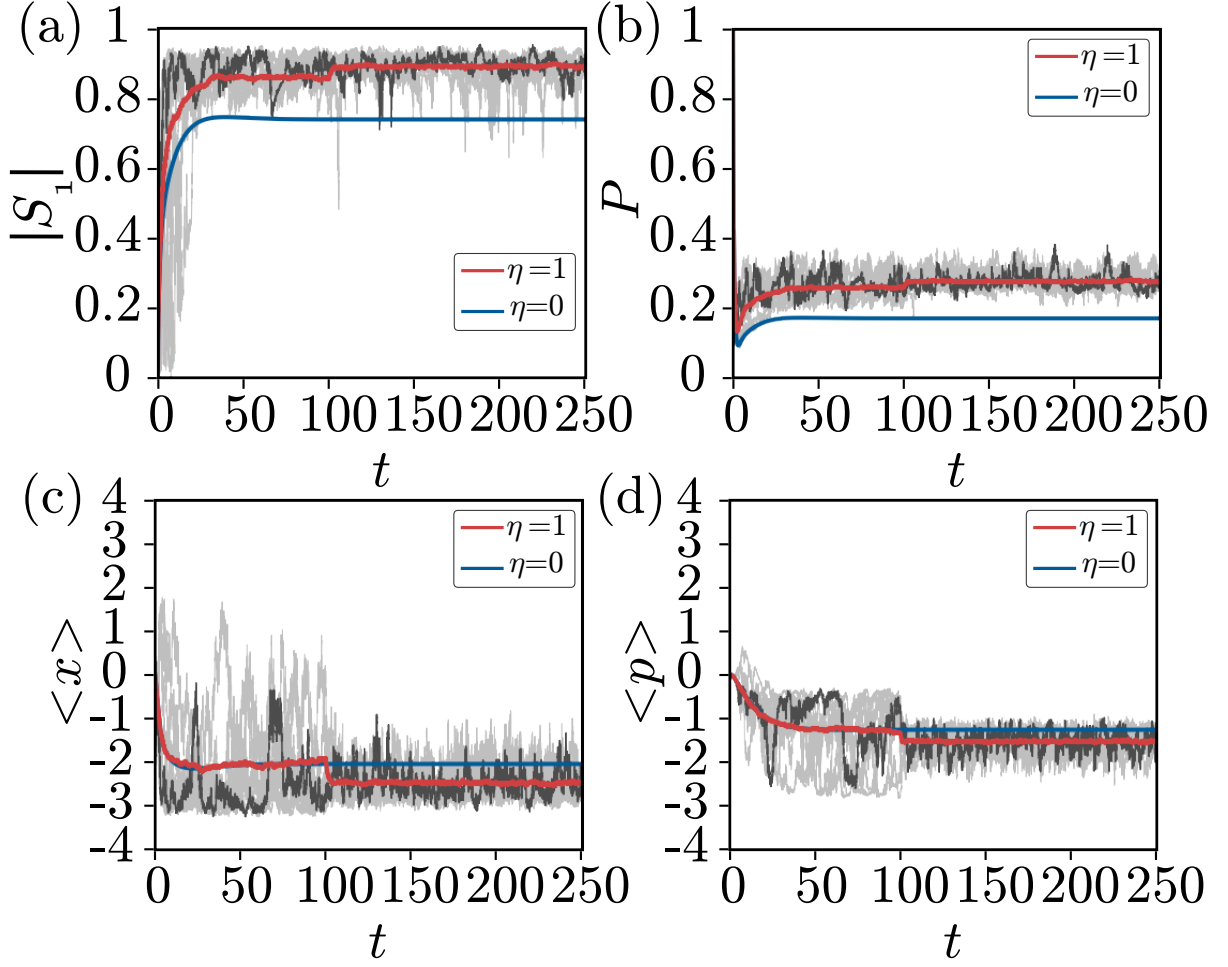


FIG. 4. Measurement-induced enhancement of quantum synchronization with feedback control in semiclassical regime. Feedback control is applied from  $t = 100$ . (a) Order parameter  $|S_1|$ . (b) Purity  $P$ . (c) Expectation values of the position operator  $\langle x \rangle$ . (d) Expectation values of the momentum operator  $\langle p \rangle$ . For the case with measurement ( $\eta = 1$ ), average values of results calculated from 300 trajectories are shown by red lines and 10 out of 300 individual trajectories are shown by gray lines with the dark one representing a single realization of the trajectory. For the case without measurement ( $\eta = 0$ ), the results of a single trajectory are shown by blue lines.

#### D. Applicability in stronger quantum regime

Finally, we discuss the enhancement of quantum synchronization via continuous measurement and feedback control in a stronger quantum regime. The parameters are shown at the beginning of Section III. Figures 7(a), 7(b), 7(c), and 7(d) show the trajectories of  $|S_1|$ ,  $P$ ,  $\langle x \rangle$ , and  $\langle p \rangle$ , respectively. The feedback control is applied after  $t = 100$ .

As shown in Fig. 7(a), the average order parameter  $|S_1|$  with measurement takes larger values than  $|S_1|$  without measurement, e.g.,  $|S_1| = 0.687$  with measurement and  $|S_1| = 0.586$  without measurement at  $t = 250$ . We also see in Fig. 7(b) that the averaged values of  $P$  with measurement are larger than the values of  $P$  without measurement, e.g.,  $P = 0.340$  with measurement and  $P = 0.266$  without measurement at  $t = 250$ .

As shown from the results above, both  $|S_1|$  and  $P$  increase on average with measurement even in this quantum regime. The suppression of the measurement-induced fluctuations by the feedback control is shown in Fig. 7(c), where 10 trajectories of  $\langle x \rangle$  obtained by simulating Eq. (1) with measurement are shown (gray lines). We see that the fluctuations in  $\langle x \rangle$  around the phase-locking point are suppressed by the feedback control which is turned on after  $t = 100$ . However, in Fig. 7(d) where 10 trajectories of  $\langle p \rangle$  obtained by simulating Eq. (1) with measurement are shown (gray lines), the fluctuations in  $\langle p \rangle$  still remain and can be even stronger after the feedback control is turned on at  $t = 100$ . We note that the fluctuations in  $\langle p \rangle$  become smaller on average but  $\langle p \rangle$  also exhibits occasional bursty

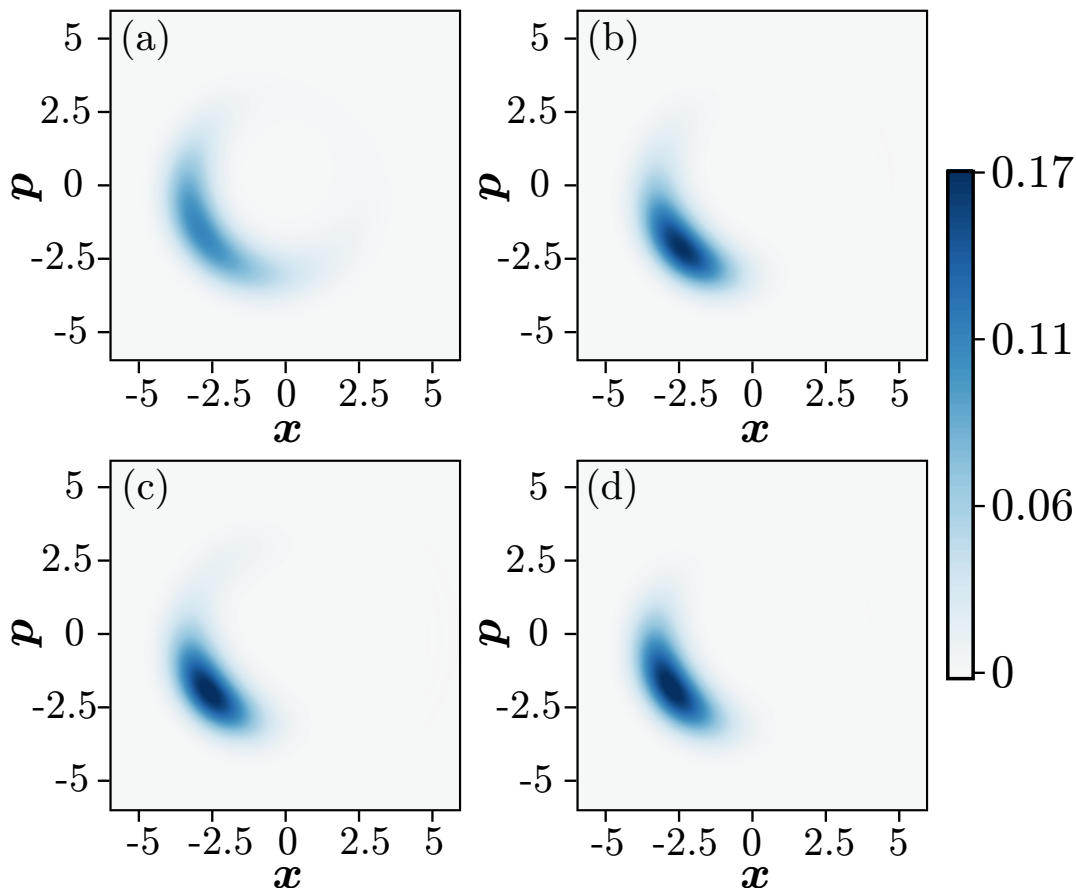


FIG. 5. Wigner distributions of system with feedback control in semiclassical regime. (a) Wigner distribution of steady state of Eq. (1) without measurement. (b,c,d) Wigner distributions of three different trajectories of Eq. (1) with measurement at  $t = 250$ . Feedback control is applied from time  $t = 100$ .

increases when the feedback control is applied. This is because the feedback control induces more localized states with stronger phase coherence than the case without feedback, and measurement-induced fluctuations of such states yield larger variations in  $\langle p \rangle$ .

These results are also observed from the Wigner distribution of the system. Figure 8(a) shows the steady-state Wigner distribution of Eq. (1) without measurement and Figs. 8(b), 8(c), and 8(d) show three realizations of the Wigner distributions at  $t = 250$  of Eq. (1) with measurement, respectively. The fluctuations around the phase-locking point are suppressed effectively by the feedback control, and the enhancement of quantum synchronization is achieved, in Figs. 8(b) and 8(c). However, the measurement-induced fluctuation remains and the phase coherence of the oscillator is decreased in Fig. 8(d).

These results indicate that quantum synchronization is enhanced only probabilistically in the strong quantum regime considered here. From the numerical results shown in Figs. 7 and 8, we empirically obtain a probability of success approximately 80 percents for the enhancement of quantum synchronization, namely, Wigner distributions at time  $t = 250$  are strongly localized around the phase-locking point  $\theta_0$  for approximately 80 percent of the trajectories. In this regime, because of the strong quantum fluctuations, the feedback control occasionally fails to suppress the measurement-induced fluctuations and enhance quantum synchronization.

We also note that the strong quantum fluctuations lead to the weaker enhancement of synchronization. This is evident in the improvement of  $|S_1| = 0.687$  from  $|S_1| = 0.586$  by a factor  $0.687/0.586 = 1.172$  in the quantum regime, which is smaller than the improvement of  $|S_1| = 0.889$  from  $|S_1| = 0.737$  by a factor  $0.889/0.737 = 1.206$  in the semiclassical regime in Figs. 4 and 5. More detailed and systematic numerical analysis in the strong quantum regime is the subject of future study.

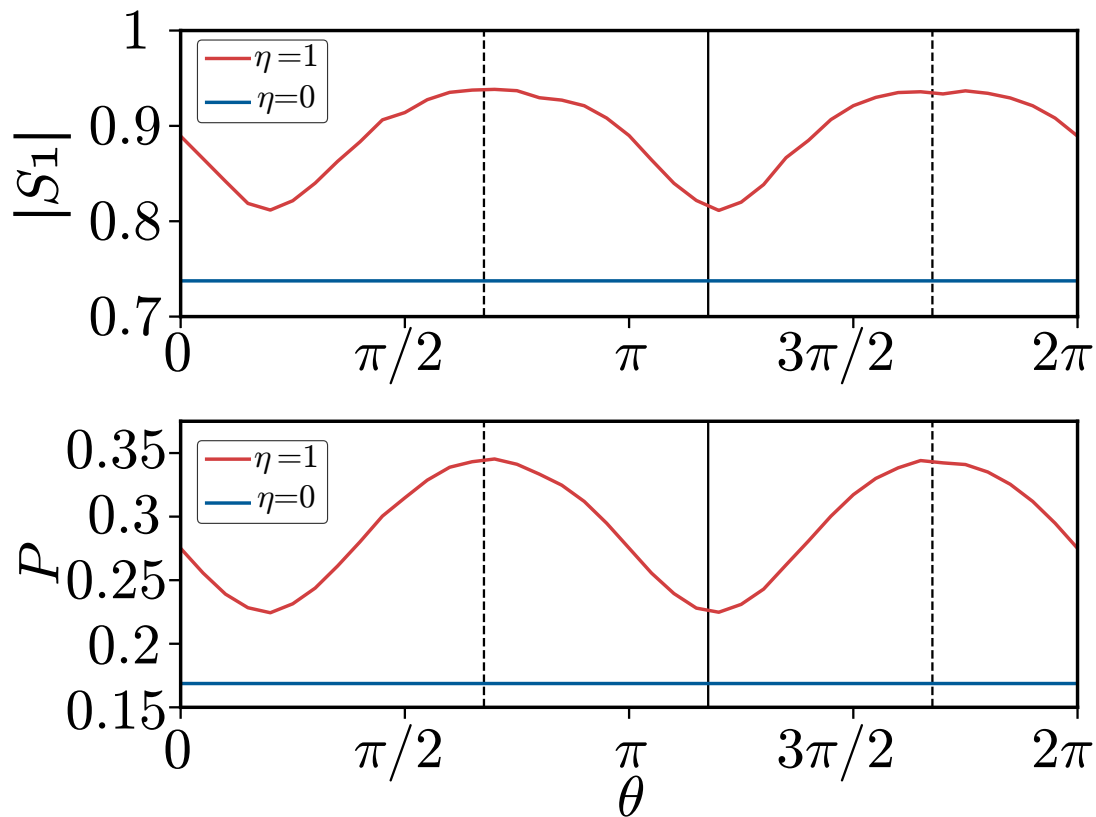


FIG. 6. Dependence of results on measurement quadrature. (a) Order parameter  $|S_1|$ . (b) Purity  $P$ . Order parameter and purity averaged over 400 trajectories with measurement at  $t = 250$  (red lines) are compared with those for a single trajectory without measurement (blue lines). Phase-locking point  $\theta_0$  (a solid black vertical line) and points orthogonal to the phase-locking point  $\theta_0 + \pi/2$  (dotted black vertical lines) are shown.

#### IV. CONCLUSION

We considered synchronization of a quantum van der Pol oscillator with a harmonic drive. We demonstrated that introducing an additional linear bath coupled to the system and performing continuous homodyne measurement of the bath can increase the phase coherence of the system. We also proposed a simple feedback policy for suppressing the fluctuations in the system state around the phase-locking point by adjusting the frequency of the harmonic drive, and achieved the measurement-induced enhancement of synchronization. We further demonstrated that the maximum enhancement of synchronization is achieved when we perform measurement on the quadrature angle at which the phase diffusion of the oscillator is maximized and the maximum information regarding the oscillator phase is attained. Finally, we demonstrated that the enhancement of quantum synchronization via continuous measurement and feedback control can be achieved with a high probability of success even in the stronger quantum regime.

The proposed system can, in principle, be implemented using the current experimental setups; synchronization of a quantum vdP with a harmonic drive can be experimentally implemented using optomechanical systems [23] or ion traps [22], and the feedback control can be implemented by adjusting the frequency of the harmonic drive using the measurement outcomes. Quantum measurement, an essential feature in quantum systems, helps us resolve the issue of quantum fluctuations that disturb strict quantum synchronization and is important for the realization and future applications of quantum synchronization in the evolving field of quantum technologies.

*Acknowledgments.*— Numerical simulations are performed using the QuTiP numerical toolbox [61]. The authors gratefully thank N. Yamamoto for the stimulating discussions. We acknowledge JSPS KAKENHI JP17H03279, JP18H03287, JPJSBP120202201, JP20J13778, and JST CREST JP-MJCR1913 for financial support.

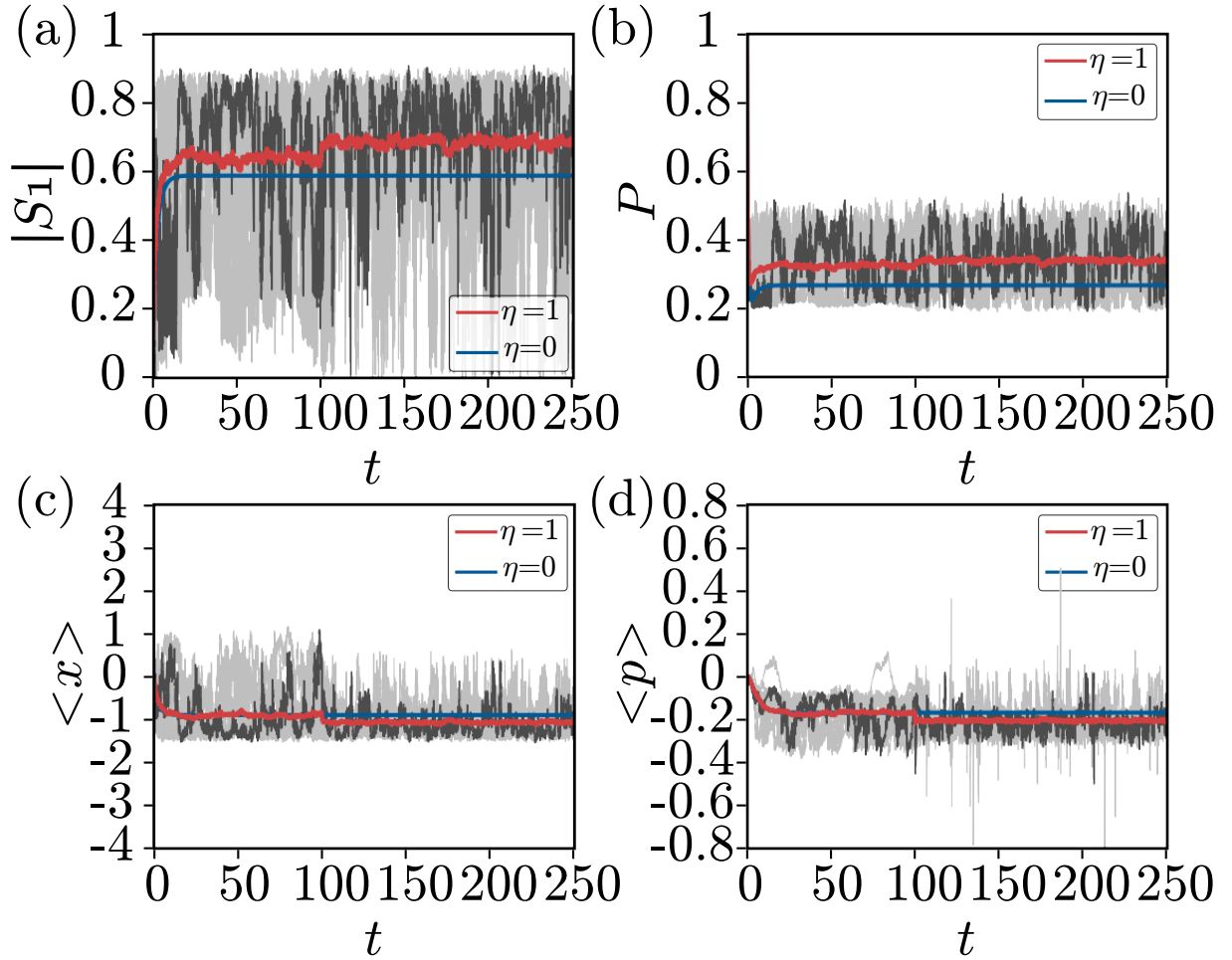


FIG. 7. Measurement-induced enhancement of quantum synchronization with feedback control in quantum regime. Feedback control is applied from  $t = 100$ . (a) Order parameter  $|S_1|$ . (b) Purity  $P$ . (c) Expectation values of position operator  $\langle x \rangle$ . (d) Expectation values of momentum operator  $\langle p \rangle$ . For the case with measurement ( $\eta = 1$ ), averaged values of results calculated from 300 trajectories are shown by red lines, and 10 out of 300 individual trajectories are shown by gray lines with the dark one representing a single realization of the trajectory. For the case without measurement ( $\eta = 0$ ), results of a single trajectory are shown by blue lines.

### 1. Feedback policy

We discuss the feedback policy for suppressing measurement-induced fluctuations around the phase-locking point. To understand the core idea of the feedback policy with a simple model, we consider the system described in Eq. (1) without the linear coupling to the bath, i.e.  $\gamma_3 = 0$ . We also assume that the system is in the semiclassical regime and the oscillator dynamics can be described by a semiclassical stochastic differential equation (SDE) whose deterministic part possesses a stable limit-cycle solution. We can then apply the semiclassical phase reduction [26] to obtain an approximate one-dimensional SDE for the phase variable of the oscillator and use the standard classical methods for the phase equation [1–5] to analyze synchronization dynamics of the oscillator driven by a periodic forcing.

When the quantum noise is sufficiently weak and the classical limit can be taken, the deterministic phase equation for the oscillator is expressed as (see also the next section) [23, 26]

$$\frac{d\phi}{dt} = \Delta + \Delta_{fb} + \sqrt{\frac{2\gamma_2}{\gamma_1}} E \sin \phi. \quad (4)$$

When  $|\Delta + \Delta_{fb}| \leq \sqrt{\frac{2\gamma_2}{\gamma_1}} E$ , there exists a stable fixed point of Eq. (4), which corresponds to the phase-locking point

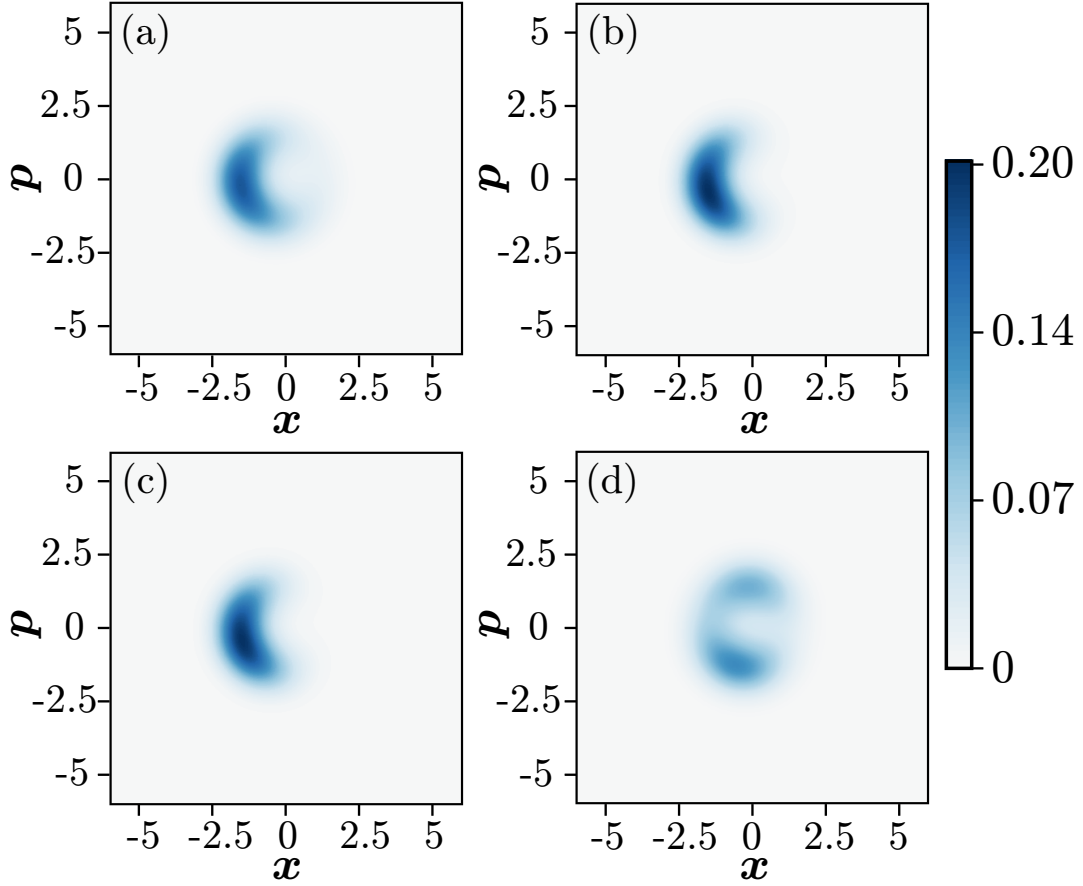


FIG. 8. Wigner distributions of system with feedback control in quantum regime. (a) Wigner distribution of steady state of Eq. (1) without measurement. (b,c,d) Wigner distributions of three different trajectories of Eq. (1) with measurement at  $t = 250$ . Feedback control is applied from time  $t = 100$ .

of the system with the harmonic driving signal under the feedback control, satisfying

$$\phi_{fb} = -\arcsin\left(\frac{\Delta + \Delta_{fb}}{E} \sqrt{\frac{\gamma_1}{2\gamma_2}}\right). \quad (5)$$

The fixed point when the feedback control is turned off, i.e.,  $\Delta_{fb} = 0$ , is expressed as

$$\phi_0 = -\arcsin\left(\frac{\Delta}{E} \sqrt{\frac{\gamma_1}{2\gamma_2}}\right). \quad (6)$$

Figure 9 shows a schematic diagram of the feedback policy for suppressing fluctuations around the phase-locking point. As shown in Fig. 9, when  $\theta_{est} > \theta_0$ , the feedback control is  $\Delta_{fb} = -K_{fb}(\theta_{est} - \theta_0) < 0$  and hence  $\phi_{fb} < \phi_0$ . Similarly, when  $\theta_{est} < \theta_0$ , we obtain  $\phi_{fb} > \phi_0$ . Therefore, the feedback control shifts the locking phase from  $\phi_0$  to  $\phi_{fb}$ , which is opposite to the direction from  $\theta_0$  to  $\theta_{est}$ , and is expected to suppress the fluctuations of the system around the phase-locking point.

## 2. Relationship between the phase diffusion and purity

We discuss the relation between the phase diffusion and purity of the quantum vdP oscillator when the measurement is absent. We consider the system described in Eq. (1) without the linear coupling to the bath, i.e.,  $\gamma_3 = 0$ ; additionally, we assume that the system is in the semiclassical regime and driven by the weak perturbation. The system can then be approximately described by a SDE of the phase variable of the oscillator by using the semiclassical phase reduction theory [26].

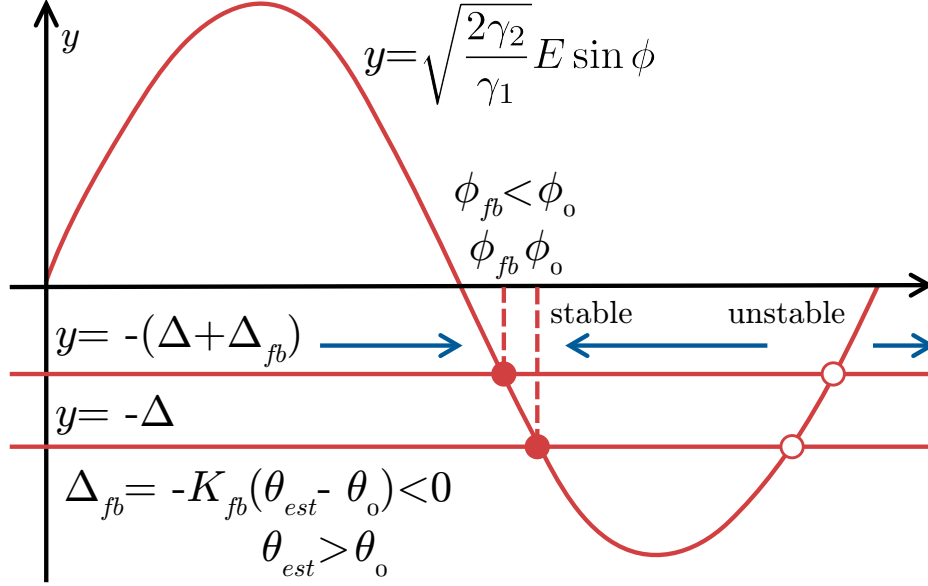


FIG. 9. Schematic diagram of feedback policy for suppressing fluctuations around phase-locking point. Feedback control shifts phase-locking point from  $\phi_0$  to  $\phi_{fb}$  that is opposite to the direction from  $\theta_0$  to  $\theta_{est}$ .

We introduce the following rescaled quantities:  $\gamma_2 = \sigma\gamma_1\gamma_2'$ ,  $\Delta + \Delta_{fb} = \gamma_1(\Delta' + \Delta'_{fb})$ ,  $E = \epsilon\gamma_1 E'/\sqrt{\sigma}$ ,  $dt' = \gamma_1 dt$ ,  $dW' = \sqrt{\gamma_1} dW$  with dimensionless parameters  $\gamma_2'$ ,  $\Delta'$ ,  $\Delta'_{fb}$ , and  $E'$  of  $\mathcal{O}(1)$ . We set  $0 < \sigma \ll 1$  (the system is in the semiclassical regime) and  $0 < \epsilon \ll 1$  (the perturbation is weak). The corresponding semiclassical phase equation for the quantum system in Eq. (1) is then given by [26]

$$d\phi = \left( \Delta' + \Delta'_{fb} + \epsilon\sqrt{2\gamma_2'} E' \sin\phi \right) dt' + \sqrt{\sigma D_0} dW', \quad (7)$$

with  $D_0 = \frac{3\gamma_2'}{2}$ .

We first evaluate the phase diffusion of the oscillator based on the effective diffusion constant of Eq.(7) [62],

$$D_{eff} \propto \frac{1}{\langle \exp(v(\phi)/(\sigma D_0)) \rangle_\phi \langle \exp(-v(\phi)/(\sigma D_0)) \rangle_\phi}, \quad (8)$$

where the potential  $v(\phi)$  is given by  $v(\phi) = -\int_{\phi_0}^{\phi} (\Delta' + \Delta'_{fb} + \epsilon\sqrt{2\gamma_2'} E' \sin\phi') d\phi'$  with a reference phase point  $\phi_0$  and  $\langle \cdot \rangle_\phi = \frac{1}{2\pi} \int_0^{2\pi} (\cdot) d\phi$ . When  $\sigma$  is sufficiently small, using the saddle-point approximation  $\langle \exp(v(\phi)/(\sigma D_0)) \rangle_\phi \approx \exp(v_{max}/(\sigma D_0))$  and  $\langle \exp(-v(\phi)/(\sigma D_0)) \rangle_\phi \approx \exp(-v_{min}/(\sigma D_0))$ , the effective diffusion constant can be approximated as

$$D_{eff} \approx \frac{1}{\exp((v_{max} - v_{min})/(\sigma D_0))}, \quad (9)$$

where  $v_{max}$  and  $v_{min}$  are the maximum and minimum values of the potential  $v(\phi)$ , respectively (see [63] for details), and the constant factors are omitted.

We next evaluate the purity. Using semiclassical phase reduction theory [26], the density matrix can be approximately reconstructed from the phase equation as  $\rho \approx \int_0^{2\pi} d\phi P(\phi) |\alpha_0(\phi)\rangle \langle \alpha_0(\phi)|$ , where  $\alpha_0(\phi) = \sqrt{\frac{1}{2\sigma\gamma_2'}} \exp(i\phi)$  is the system state at  $\phi$  on the classical limit cycle in the phase space of the P representation [60] and  $P(\phi)$  is the steady-state probability distribution of the Fokker-Planck equation for the phase variable given by ([3], Chapter 9)

$$P(\phi) \propto \int_0^{2\pi} d\phi' \exp \left[ \frac{2(v(\phi' + \phi) - v(\phi))}{\sigma D_0} \right]. \quad (10)$$

Because the size of the limit cycle is  $O(1/\sqrt{\sigma})$ , i.e.,  $\alpha_0(\phi) = O(1/\sqrt{\sigma})$ , when  $\sigma$  is sufficiently small, the purity can be evaluated by using saddle-point approximation as

$$\begin{aligned} P &= \text{Tr}(\rho^2) \approx \int_0^{2\pi} d\phi P(\phi) \int_0^{2\pi} d\phi' P(\phi') \exp(-|\alpha_0(\phi) - \alpha_0(\phi')|^2) \\ &\approx \int_0^{2\pi} d\phi P^2(\phi) \approx \int_0^{2\pi} d\phi \left( \int_0^{2\pi} d\phi' \exp\left[\frac{2(v(\phi') + \phi) - v(\phi)}{\sigma D_0}\right] \right)^2 \\ &\approx \int_0^{2\pi} d\phi \left( \exp\left[\frac{2(v_{max} - v(\phi))}{\sigma D_0}\right] \right)^2 \approx \exp\left[\frac{4(v_{max} - v_{min})}{\sigma D_0}\right], \end{aligned}$$

where the constant factors are omitted. The effective diffusion constant  $D_{eff}$  can then be approximately represented as

$$D_{eff} \propto \frac{1}{(P)^{1/4}}, \quad (11)$$

which indicates that a higher purity results in a smaller phase diffusion of the oscillator.

- 
- [1] A. T. Winfree, *The geometry of biological time* (Springer, New York, 2001).  
[2] Y. Kuramoto, *Chemical oscillations, waves, and turbulence* (Springer, Berlin, 1984).  
[3] A. Pikovsky, M. Rosenblum, and J. Kurths, *Synchronization: a universal concept in nonlinear sciences* (Cambridge University Press, Cambridge, 2001).  
[4] H. Nakao, *Contemporary Physics* **57**, 188 (2016).  
[5] S. Strogatz, *Nonlinear dynamics and chaos* (Westview Press, 1994).  
[6] S. Shapiro, *Physical Review Letters* **11**, 80 (1963).  
[7] R. Adler, *Proceedings of the IRE* **34**, 351 (1946).  
[8] R. E. Best, *Phase-locked loops: theory, design, and applications* (McGraw-Hill, New York, 1984).  
[9] P. A. Tass, *Biological Cybernetics* **85**, 343 (2001).  
[10] S. Shim, M. Imboden, and P. Mohanty, *Science* **316**, 95 (2007).  
[11] M. Zhang, G. S. Wiederhecker, S. Manipatruni, A. Barnard, P. McEuen, and M. Lipson, *Physical Review Letters* **109**, 233906 (2012).  
[12] M. Zhang, S. Shah, J. Cardenas, and M. Lipson, *Physical Review Letters* **115**, 163902 (2015).  
[13] M. Bagheri, M. Poot, L. Fan, F. Marquardt, and H. X. Tang, *Physical Review Letters* **111**, 213902 (2013).  
[14] M. H. Matheny, M. Grau, L. G. Villanueva, R. B. Karabalin, M. Cross, and M. L. Roukes, *Physical Review Letters* **112**, 014101 (2014).  
[15] M. H. Matheny, J. Emenheiser, W. Fon, A. Chapman, A. Salova, M. Rohden, J. Li, M. H. de Badyn, M. Pósfai, L. Duenas-Osorio, *et al.*, *Science* **363**, eaav7932 (2019).  
[16] S. Kreinberg, X. Porte, D. Schicke, B. Lingnau, C. Schneider, S. Höfling, I. Kanter, K. Lüdge, and S. Reitzenstein, *Nature communications* **10**, 1539 (2019).  
[17] H. Singh, S. Bhuktare, A. Bose, A. Fukushima, K. Yakushiji, S. Yuasa, H. Kubota, and A. A. Tulapurkar, *Physical Review Applied* **11**, 054028 (2019).  
[18] M. Colombano, G. Arregui, N. Capuj, A. Pitanti, J. Maire, A. Griol, B. Garrido, A. Martinez, C. Sotomayor-Torres, and D. Navarro-Urrios, *Physical Review Letters* **123**, 017402 (2019).  
[19] C.-G. Liao, R.-X. Chen, H. Xie, M.-Y. He, and X.-M. Lin, *Physical Review A* **99**, 033818 (2019).  
[20] A. W. Laskar, P. Adhikary, S. Mondal, P. Katiyar, S. Vinjanampathy, and S. Ghosh, *Physical Review Letters* **125**, 013601 (2020).  
[21] M. Koppenhöfer, C. Bruder, and A. Roulet, *Physical Review Research* **2**, 023026 (2020).  
[22] T. E. Lee and H. Sadeghpour, *Physical Review Letters* **111**, 234101 (2013).  
[23] S. Walter, A. Nunnenkamp, and C. Bruder, *Physical Review Letters* **112**, 094102 (2014).  
[24] T. E. Lee, C.-K. Chan, and S. Wang, *Physical Review E* **89**, 022913 (2014).  
[25] S. Sonar, M. Hajdušek, M. Mukherjee, R. Fazio, V. Vedral, S. Vinjanampathy, and L.-C. Kwek, *Physical Review Letters* **120**, 163601 (2018).  
[26] Y. Kato, N. Yamamoto, and H. Nakao, *Phys. Rev. Research* **1**, 033012 (2019).  
[27] Y. Kato and H. Nakao, *Physical Review E* **101**, 012210 (2020).  
[28] Y. Kato and H. Nakao, arXiv preprint arXiv:2006.00760 (2020).  
[29] T. Weiss, A. Kronwald, and F. Marquardt, *New Journal of Physics* **18**, 013043 (2016).  
[30] N. Es' haqi Sani, G. Manzano, R. Zambrini, and R. Fazio, *Physical Review Research* **2**, 023101 (2020).  
[31] A. Roulet and C. Bruder, *Physical Review Letters* **121**, 053601 (2018).  
[32] N. Lörch, E. Amitai, A. Nunnenkamp, and C. Bruder, *Physical Review Letters* **117**, 073601 (2016).

- [33] S. Walter, A. Nunnenkamp, and C. Bruder, *Annalen der Physik* **527**, 131 (2015).
- [34] V. Bastidas, I. Omelchenko, A. Zakharova, E. Schöll, and T. Brandes, *Physical Review E* **92**, 062924 (2015).
- [35] M. Ludwig and F. Marquardt, *Physical Review Letters* **111**, 073603 (2013).
- [36] M. R. Hush, W. Li, S. Genway, I. Lesanovsky, and A. D. Armour, *Physical Review A* **91**, 061401 (2015).
- [37] A. Roulet and C. Bruder, *Physical Review Letters* **121**, 063601 (2018).
- [38] N. Lörch, S. E. Nigg, A. Nunnenkamp, R. P. Tiwari, and C. Bruder, *Physical Review Letters* **118**, 243602 (2017).
- [39] E. Amitai, N. Lörch, A. Nunnenkamp, S. Walter, and C. Bruder, *Physical Review A* **95**, 053858 (2017).
- [40] M. Xu, D. A. Tieri, E. Fine, J. K. Thompson, and M. J. Holland, *Physical Review Letters* **113**, 154101 (2014).
- [41] M. Xu and M. Holland, *Physical Review Letters* **114**, 103601 (2015).
- [42] D. Witthaut, S. Wimberger, R. Burioni, and M. Timme, *Nature Communications* **8**, 14829 (2017).
- [43] T. Weiss, S. Walter, and F. Marquardt, *Physical Review A* **95**, 041802 (2017).
- [44] C. Davis-Tilley, C. Teoh, and A. Armour, *New Journal of Physics* **20**, 113002 (2018).
- [45] J. von Neumann, *Mathematical Foundations of Quantum Mechanics* (Springer, 1932).
- [46] M. A. Nielsen and I. L. Chuang, *Quantum Computation and Quantum Information* (Cambridge University Press, 2000).
- [47] V. P. Belavkin, *Journal of Multivariate analysis* **42**, 171 (1992).
- [48] H. M. Wiseman and G. J. Milburn, *Quantum measurement and control* (Cambridge University Press, 2009).
- [49] K. Jacobs, *New Journal of Physics* **12**, 043005 (2010).
- [50] Y. Kato and N. Yamamoto, *New Journal of Physics* **16**, 023024 (2014).
- [51] M. Gu, A. Parkins, and H. Carmichael, *Physical Review A* **73**, 043813 (2006).
- [52] T. Bhattacharya, S. Habib, and K. Jacobs, *Physical Review Letters* **85**, 4852 (2000).
- [53] A. Scott and G. J. Milburn, *Physical Review A* **63**, 042101 (2001).
- [54] J. K. Eastman, S. S. Szigeti, J. J. Hope, and A. R. Carvalho, *Physical Review A* **99**, 012111 (2019).
- [55] M. Hatridge, S. Shankar, M. Mirrahimi, F. Schackert, K. Geerlings, T. Brecht, K. Sliwa, B. Abdo, L. Frunzio, S. M. Girvin, *et al.*, *Science* **339**, 178 (2013).
- [56] Z. Mineev, S. Mundhada, S. Shankar, P. Reinhold, R. Gutiérrez-Jáuregui, R. Schoelkopf, M. Mirrahimi, H. Carmichael, and M. Devoret, *Nature* **570**, 200 (2019).
- [57] M. Hays, V. Fatemi, K. Serniak, D. Bouman, S. Diamond, G. de Lange, P. Krogstrup, J. Nygård, A. Geresdi, and M. Devoret, *Nature Physics*, 1 (2020).
- [58] M. Koppenhöfer, C. Bruder, and N. Lörch, *Physical Review A* **97**, 063812 (2018).
- [59] Y. Kato and H. Nakao, "Instantaneous quantum phase synchronization of two decoupled quantum limit-cycle oscillators induced by conditional photon detection", in preparation.
- [60] C. W. Gardiner, *Quantum Noise* (Springer, New York, 1991).
- [61] J. Johansson, P. Nation, and F. Nori, *Computer Physics Communications* **183**, 1760 (2012); **184**, 1234 (2013).
- [62] S. Lifson and J. L. Jackson, *The Journal of Chemical Physics* **36**, 2410 (1962).
- [63] A. Pikovsky, *Physical Review Letters* **115**, 070602 (2015).